

Learning to Charge RF-Energy Harvesting Devices in WiFi Networks

Yizhou Luo and Kwan-Wu Chin

Abstract—In this paper, we consider a solar-powered Access Point (AP) that is tasked with supporting both non-energy harvesting or *legacy* data users such as laptops, and devices with Radio Frequency (RF)-energy harvesting and sensing capabilities. We propose two solutions that enable the AP to manage its harvested energy via transmit power control and also ensure devices perform sensing tasks frequently. Advantageously, our solutions are suitable for current wireless networks and do not require perfect channel gain information or non-causal energy arrival at devices. The first solution uses a deep Q-network (DQN) whilst the second solution uses Model Predictive Control (MPC) to control the AP's transmit power. Our results show that our DQN and MPC solutions improve energy efficiency and user satisfaction by respectively 16% to 35%, and 10% to 42% as compared to competing algorithms.

Index Terms—Wireless Charging, Reinforcement Learning, Receding Horizon Control, Regression, Energy Allocation.

I. INTRODUCTION

The Internet of Things (IoT) network [1] will play a critical role in our daily activities. In particular, sensing devices will be an integral part of devices purchased by consumers. For example, as detailed in [2], wearable devices with sensing capabilities such as a thermometer, video camera or smart watch are now available commercially to enable smart homes/offices as well as for video surveillance. Another example is [3], whereby a motion sensor is used to infer usage of appliances in a home. Moreover, these devices are likely to harvest energy from Wireless Local Area Networks (WLANs), which are now ubiquitous and widely used to connect conventional IEEE 802.11 devices such as iPads [2]. Energy efficiency is also becoming a concern [4]. To this end, future WLANs are likely to incorporate Energy Harvesting (EH) Access Points (APs) in order to reduce carbon emissions and operating expenditure [5]. Moreover, IoT devices will have Radio Frequency (RF)-energy harvesting capability; see [6] for a prototype that uses transmissions from an AP to power an on-board camera.

Figure 1 shows a solar-powered AP that serves not only *legacy* data users/devices, which do not have RF-energy harvesting capability, but also nearby IoT devices equipped with a temperature sensor and an RF-energy harvester. All nodes operate on the *same* frequency. Whenever the AP delivers data to *legacy* users, IoT devices harvest RF-energy. The amount of harvested RF-energy is a function of their distance to the AP, time-varying channel gains, how often the AP transmits and also the AP's transmit power; Figure 1 shows two possible transmit power levels. A key challenge here is that the transmit

power used by the AP is dependent on its available energy, which exhibits spatio-temporal properties. Critically, the AP only has *causal* knowledge of its solar energy arrivals; i.e., the AP only knows its current and past energy arrivals. Another challenge is that IoT devices may be tasked with returning their sample data periodically. However, they may not have harvested sufficient energy from the AP's data transmissions.

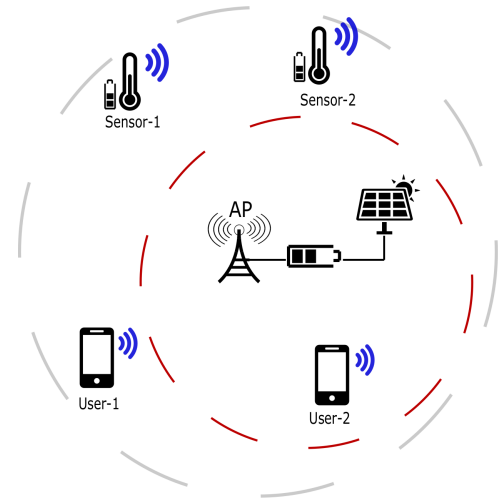


Fig. 1. An example network with a solar-powered AP and both legacy data users and RF-energy harvesting IoT devices. Both sensors receive energy whenever the AP uses a high transmit power level, denoted by the gray circle.

Henceforth, our aim is to determine a transmit power allocation policy that allows an AP to support the data rate of *legacy* data users, and at the same time delivers RF-energy to IoT devices. In this respect, this paper contains the following contributions. We present two solutions to derive the said policy and compare their performance in improving user satisfaction. The first solution relies on the Deep Q-Network (DQN) framework, where given an AP's state comprising of its energy level and legacy user channel gain, it determines the best transmit power control that yields the maximum satisfaction for both user types. The second solution uses Model Predictive Control (MPC), where the AP uses Gaussian Process Regression (GPR), a machine learning method, to predict future harvested energy and channel gains. Both solutions do not rely on perfect Channel State Information (CSI) to IoT devices and assume causal energy arrivals at the AP. These assumptions are made for practical reasons to ensure our solutions are readily deployable in current wireless networks.

Next, in Section II, we identify gaps in past works. Section III formalizes our system and problem. After that

The authors are with the School of Electrical, Computer and Telecommunications Engineering, University of Wollongong, NSW, Australia. Email: yl631@uowmail.edu.au, kwanwu@uow.edu.au

Section IV outlines two solutions and they are evaluated in Section V. Section VI concludes the paper.

II. RELATED WORKS

Numerous works have considered RF-charging or Wireless Powered Communication Networks (WPCNs); see [7] and references therein. They mainly focus on maximizing the sum-rate at an Hybrid Access Point (HAP) [8], [9]. However, they mostly consider optimizing charging and transmission slots, which is different to our problem. Our work overlaps with those that apply Reinforcement Learning (RL) to adjust the transmission power of an HAP. For example, in [10], the goal is for a HAP to learn a robust transmission/changing power control policy to minimize the number of dropped packets due to attacks. These works, however, only consider one type of users; namely RF-energy devices. Also, their HAP does not harvest energy. Critically, they assume the current channel condition of devices is known by HAPs. We do not make such assumptions. Another group of works considers EH HAPs [11], [12] to charge RF-energy devices. They aim to transfer energy to RF devices in order to maximize the sum-rate or lifetime of devices. In [11], the authors determine the transmission power of HAPs and control the active/sleep modes of HAPs. The aim is to maximize the lifetime of IoT devices given casual energy arrivals at a HAP. In [12], the authors propose to manage the energy consumption of HAPs for tasks such as sensing, computing, and uplink transmission. The aim is to minimize the average consumption of on-grid energy while ensuring IoT devices have sufficient energy or capacity. However, their system is different from ours because we consider RF changing in an existing WiFi systems.

To date, only a small number of works have considered supporting two types of users; namely, [6], [13], [14], [15]. In [6], APs inject a power packet whenever their data queue length is shorter than a given number of packets. Reference [13] aims to optimize the transmissions of APs in order to i) maximize the amount of energy delivered to an RF sensor, and ii) minimize the total number of packets queued at APs. In [14], the authors study the impact of interference on both data users and RF-energy users. The authors aim to optimize sub-carrier allocation and transmission power control in order to minimize the total energy consumption of their system. Reference [15] aims to determine the beacon frequency of an AP and the charging period of IoT devices that maximize their lifetime. Our work is fundamentally different to these works. First, the APs or base stations of these works have no EH capability. Second, our work aims to control the transmission power at an AP with stochastic energy arrivals in order to satisfy both RF-energy devices and legacy WiFi users. Another distinction to prior works is that we consider imperfect CSI to IoT devices and causal knowledge of energy arrivals. Moreover, they use mathematical optimization as a solution approach and requires non-causal information. On the other hand, we employ machine learning approaches and adapt to historical CSI and energy arrivals.

III. SYSTEM MODEL AND PROBLEM

We assume time is discrete, and the set of time slots is $\mathcal{T} = \{1, 2, \dots, T\}$. Each slot is one second in length; this means the term power and energy can be used interchangeably. There are N IoT devices uniformly located around an AP. Let \mathbb{D} be the set of IoT devices. Similarly, there are U legacy data users. In each time slot, the AP serves one data user.

The AP has a battery of size B_{max} . Its energy arrival is governed by the Markovian model presented in [16]. Specifically, the model contains four different solar states: ‘Excellent’, ‘Good’, ‘Fair’, and ‘Poor’. Each state represents different solar intensity throughout a day. In the j -th state, the energy arrival x (in mJ) is a random value drawn from a Normal distribution $\mathcal{N}(x | \mu_j, \sigma_j)$ with mean μ_j and variance σ_j . Then, the energy harvested by the AP in slot t is $\tilde{E}_t = x_t \Phi \bar{\eta}$, where Φ and $\bar{\eta}$ is the panel size and the solar energy conversion efficiency. The energy level of the AP, denoted as B_t , evolves as per,

$$B_t = \min(B_{max}, B_{t-1} - P_{t-1} + \tilde{E}_t), \quad (1)$$

where P_t (in mW) is the transmission power of the AP at time slot t , which is bounded by P_{max} .

We consider block fading. The AP is aware of the CSI to *legacy* or data users but is unaware of the CSI to IoT devices. Let g_i^t be the channel gain between the AP and IoT device i , and it is defined as,

$$g_i^t = \frac{1}{d_i^2} |Z|^2, \quad (2)$$

where Z is drawn from a complex normal distribution $\mathcal{CN}(\mu, \sigma^2)$, and d_i denotes the of device i from the AP.

IoT devices are equipped with a battery with capacity b_{max} . Let b_i^t be the current battery level of IoT device i . In each slot, IoT devices receive a charge whenever the AP transmits. The receive signal power p_i^t at IoT device i is calculated as $p_i^t = g_i^t P_t$. We consider a practical 2.4 GHz non-linear RF harvester [17]. For IoT device i , $\beta(p_i^t)$ returns the RF-energy conversion rate of the harvester given incident power p_i^t .

Each IoT device consumes a fixed amount of energy, denoted as \hat{E} (in mJ), to sample and return its data to the AP. If its energy level satisfies $b_i^t < \hat{E}$, device i will not carry out any operation. Mathematically, b_i^t evolves as follows,

$$b_i^t = \begin{cases} b_i^{t-1} + p_i^t \beta, & b_i^t < \hat{E}, \\ \min(b_{max}, b_i^{t-1} + p_i^t \beta - \hat{E}), & \text{Otherwise.} \end{cases} \quad (3)$$

In each time slot, the AP transmits to a random data user $u \in U$ that has a channel gain of g_u^t . Let $\gamma_u^t = p_u^t / N_0$ be the Signal-to-Noise Ratio (SNR) of user u , where p_u^t is the received signal strength and N_0 is the white noise power. As per the Shannon-Hartley formula, its data rate is,

$$r_u^t = W \log_2(1 + \gamma_u^t), \quad (4)$$

where W is the bandwidth of the channel.

Without loss of generality, we assume all users in U have a fixed data rate requirement r_{min} . Define an indicator J^t that returns one if $r_u^t \geq r_{min}$; otherwise, it returns zero. Let I^t be an indicator that returns a value of one if *all* IoT devices are able to collect a sample and transmit in slot t .

Our problem is as follows: find the optimal transmit power policy π^* that returns the transmit power level for each time t that maximizes,

$$Z_1 = \lim_{T \rightarrow \infty} \frac{1}{T} \mathbb{E} \left[\sum_{t=1}^T I^t J^t \right]. \quad (5)$$

We will also consider an alternative aim, which is to maximize energy efficiency. That is,

$$\eta_t = \begin{cases} \frac{I^t J^t}{P_t}, & P_t \neq 0, \\ 0, & P_t = 0. \end{cases} \quad (6)$$

In words, Eq. 6 represents the fact that energy efficiency is higher if the AP uses less energy to support both types of users. In this respect, the second objective is to maximize,

$$Z_2 = \lim_{T \rightarrow \infty} \frac{1}{T} \mathbb{E} \left[\sum_{t=1}^T \eta_t \right]. \quad (7)$$

IV. SOLUTIONS

We first outline our RL solution followed by a solution that uses MPC.

A. Solution-1: Reinforcement Learning

We first formulate our problem at hand as a Markov Decision Process (MDP) [18], which is then solved using a Deep Q-network (DQN) [19].

1) *MDP*: Define a tuple with four elements $(S, A, P(s_{t+1}|s_t, a_t), R(s_{t+1}|s_t, a_t))$. The state space is S , where $s_t \in S$ represents the state at time t . The term A represents the action space and $a_t \in A$ is the action taken at t . The transition probability to state s_{t+1} after taking action a_t is defined as $P(s_{t+1} | s_t, a_t)$. Lastly, the reward function $R(s_{t+1}|s_t, a_t)$ returns the immediate reward r_t after taking action a_t at state s_t . We assume there is an agent that observes the state, takes an action and then claims a reward. Let π be the policy taken by an agent, where $\pi(s_t)$ returns the action a_t when state s_t is seen. Let π^* be the optimal policy. The agents goal is to find the optimal policy π^* that maximizes the following long-term cumulative reward,

$$\mathbb{E} \left[\sum_{t=0}^{+\infty} R(s_{t+1}|s_t, \pi(s_t)) \right]. \quad (8)$$

We are now ready to instantiate an MDP for our problem. Let the state s_t be a tuple $s_t = (g_u^t, B_t)$ that includes the channel gain of a user and the battery level of the AP. The action a_t corresponds to the transmission power level P_t adopted by the AP at slot t . It has range $[0, P_{max}]$, meaning that the AP can choose a transmission power from $[0, P_{max}]$. Also, we discretize the action space equally to N_A actions. In addition, if the AP's battery B_t has insufficient energy to support the action chosen by the agent, then we encode the action to $a_t = B_t$. This means the AP consumes all the energy in its battery at slot t . As we consider two different objectives Z_1 and Z_2 , which correspond to (5) and (7), respectively, we define two reward definitions, denoted as **Reward-1** and

Reward-2. For Reward-1, the reward r_t for state s_t and action a_t is defined as $r_t = I^t J^t$. To be specific, if the AP takes an action that is able to satisfy both types of users, then the reward is one; otherwise, it is zero. The second reward definition, namely Reward-2 relate to the energy efficiency η_t achieved by the AP at slot t , and is defined as $r_t = \eta_t$. Reward-2 reveals the fact that the AP will claim more reward if it is able to achieve higher energy efficiency. Note, unless stated explicitly, our approach will apply Reward-1. The aforementioned transition of state-action-reward satisfies the Markov property. That is, the battery level in the next state s_{t+1} depends on the current state battery level and the action taken at slot t . Also, the historical battery level and channel gain do not impact the transition of the current state s_t to the next state s_{t+1} . To ensure our solution is practical, we assume the transition probability $P(s_{t+1} | s_t, a_t)$ is unknown. Hence, as our MDP is model-free. To solve the formulated MDP, we will apply an RL approach, namely, Deep Q-network (DQN) to learn the optimal policy π^* that maximizes (5) or (7).

2) *DQN*: The architecture of a DQN is shown in Figure 2. Briefly, an agent located at the AP observes the environment (state) and takes an action based on its policy. The agent consists of a set of neural networks that outputs the expected value or Q-value of actions. It then observes the resulting reward, and uses it to update its policy.

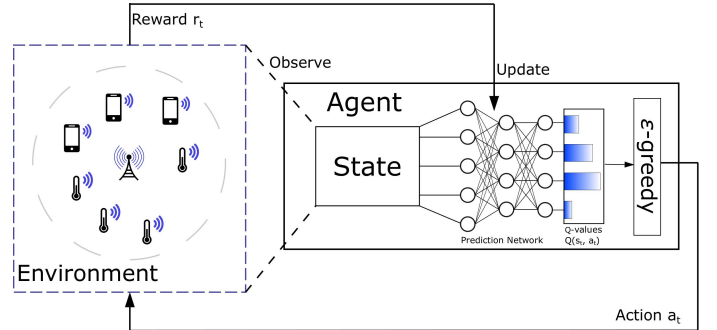


Fig. 2. An illustration of a DQN.

Let the Q-value $Q(s_t, a_t)$ denote the expected accumulated reward of a state-action after taking action a_t at state s_t . A DQN uses a neural network to estimate Q-values. To do that, it includes two sets of neural networks; one of which denoted θ is for evaluation, and the other target network is denoted as θ' . A DQN aims to minimize the temporal difference-error of Q-values, defined as,

$$L(\theta) = \min \mathbb{E}[(Q'(r_t, s_{t+1}, a_{t+1}, \theta') - Q(s_t, a_t, \theta))^2], \quad (9)$$

where $Q'(r_t, s_{t+1})$ is the targeted Q-value, given by the target network θ' and $Q(s_t, a_t, \theta)$ is the evaluated Q-value, provided by the evaluation network θ . The training data is from a memory buffer that stores historical state-action-reward pairs. For every K slots, we train our DQN using the Stochastic Gradient Descent method [20] with a learning rate α . For every K' slots, where $K' \gg K$, we copy the evaluated network θ to become a new target network θ' .

In each slot, the evaluation network θ will output the evaluated Q-value $Q(s_t, a_t, \theta)$ for each action. An agent then

selects an action using the ϵ -greedy policy. That is, it will take the action with the maximum Q-value with probability $(1-\epsilon_t)$, where ϵ is the exploration rate. Otherwise, a random action will be taken. To ensure the agent explores actions sufficiently, it uses a diminishing exploration rate, calculated as per,

$$\epsilon_t = \max \left[1, \epsilon_T + \frac{\epsilon_{inc}}{(t+1)^2} \right], \quad (10)$$

where ϵ_0 and ϵ_T are the initial and final exploration rate, respectively. The term ϵ_{inc} is the diminishing rate of ϵ_t .

B. Solution-2: MPC

Also known as Receding Horizon Control (RHC), MPC is used to choose control actions over a moving time horizon. It relies on a prediction model to predict the system dynamics, e.g., prices, weather, heating requirements. The prediction is then used to build a virtual system model that simulates the changes of a real system several slot ahead. At slot t , MPC determines an optimal control action u_t^* to maximize a performance index V_t^* over a time window $[\tau, \tau + L]$. That is,

$$V_t^* = \max \frac{1}{L+1} \sum_{\tau=t}^{t+L} v_\tau(x_\tau, u_\tau), \quad (11)$$

where L is the number of predicted time slots. The term x_τ is the predicted system state, where τ represents a time slot in a virtual system model. Note, the system states $x_{\tau+1}, \dots, x_{\tau+L}$ are the system state given by a prediction model. The term u_τ denotes the action for predicted slot τ . The instantaneous performance $v_\tau(x_\tau, u_\tau)$ depends on both the current state x_τ and control action u_τ . Eq. 11 is solved iteratively.

In our case, the system state x_t corresponds to the solar energy arrival at our AP \tilde{E}_t and channel gain of data users g_u^t and IoT devices $\{g_i^t; i = 1, \dots, N\}$. The control action u_t is the transmission power level taken by the AP, ranging from $[0, P_{max}]$. The performance index is defined as $v_\tau(\cdot) = I^\tau J^\tau$. In addition, we also define $v_\tau(\cdot) = \eta_t$ when we optimize the second objective Z_2 , see Eq. (7).

We employ Gaussian Process Regression (GPR) [21] as our prediction model. A GPR model can be trained as a probabilistic nonparametric black-box to identify a non-linear dynamic system. Given a set of training data $\{(q_i, p_i); i = 1, 2, \dots, k\}$, A GPR model is to learn the predictive response value p' for a new input value q' . A GPR model is trained using the following linear regression model,

$$p = q^T w + \xi, \quad (12)$$

where the coefficient w and the error variance $\hat{\sigma}^2$ of $\xi \sim \mathcal{N}(0, \hat{\sigma}^2)$ are learned from training data. To build our training data, we let q_i be the i -th slot and p_i be the value of a network parameter; e.g., the energy arrival at the slot i . For each network parameter, we employ an independent GPR model. As an example, consider predicting the energy arrivals at the AP using GPR. We use set D_t with size k to store the energy arrivals in last t slots; i.e., the set D_t is a shifting window for energy arrivals $\{(i, \tilde{E}_i); i = t-k, t-k-1, \dots, t\}$ in the last k slots. In each slot, we train a GPR model using the training

data in set D_t , where the input value p is time slot and the response value q is the corresponding energy arrivals.

Figure 3 illustrates our MPC solution. First, it provides training data D_t to the GPR predictor. At time slot t , the GPR predictor generates a set of system state predictions $x_{\tau+1} \dots x_{\tau+L}$, according to the current state x_t . With the predicted future states in hand, it builds a virtual system model that allows the optimizer to implement its virtual control action u_τ . The optimizer we use to solve Eq. 11 is binary search method with precision Ψ ; see [22]. Then, the virtual system model evaluates the performance $v_\tau(\cdot)$ given action u_τ . Once we have the optimal V_t^* , the optimizer will output the corresponding control action u_t^* and apply u_t^* in time slot t . Eq. 11 is then solved iteratively until $t = T$.

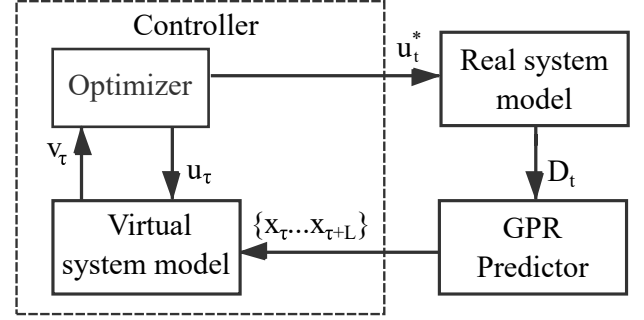


Fig. 3. An illustration of MPC.

V. EVALUATION

We conducted our simulations using Python 3.5 with TensorFlow 1.0 and Scikit-learn 0.21. Table I shows all our parameter values. We *emphasize* that as our problem is new, there are no other solutions that we can benchmark against our solutions. To this end, we benchmark DQN and MPC against the following algorithms/solutions/rules:

- **Tabular RL (TRL):** The state, action and reward are the same as that of DQN. However, the difference is that TRL uses a table to store Q-values and does not have the memory replay feature.
- **Greedy:** In every slot, the AP uses P_{max} to transmit; otherwise, it uses a transmission power level that consumes all the energy in its battery.
- **Random:** The AP uniformly chooses a transmission power level in the range $[0, P_{max}]$.
- **No-policy:** The AP is not aware of IoT devices and aims to only meet the requirement of data users. For a given data user u , the transmission power P_t is calculated as

$$P_t = \frac{N_0(2^{\frac{r_{min}}{W}} - 1)}{g_u^t}. \quad (13)$$

We assume each episode has 3,000 slots. For each episode, we calculate the average value of the following metrics:

- **Number of activated IoT devices** per slot, which is calculated as $\frac{1}{3000} \sum_{t=3000}^t n_t$. This metric corresponds to the average number of IoT devices that achieve sampling per slot in one episode.

- **Fraction of satisfied data users.** This is calculated as $\frac{1}{3000} \sum_{t+3000}^t I_t$, meaning the number of satisfied data users over one episode of slots.
- **Energy efficiency,** which is equal to $\frac{1}{3000} \sum_{t+3000}^t \eta_t$. This metric is the average energy efficiency achieved by an AP in one episode.
- **Reward.** This is defined as the average reward gained by the agent within one episode; it is calculated as $\frac{1}{3000} \sum_{t+3000}^t r_t$, where r_t refers to Reward-1.

TABLE I
PARAMETER VALUES USED IN OUR EXPERIMENTS.

Model Parameters	Values
Number of IoT Devices N	5
The minimum user distance d_{min}	5 meters
The maximum user distance d_{max}	25 meters
The minimum device distance \hat{d}_{min}	9 meters
The maximum device distance \hat{d}_{max}	10 meters
The maximum battery of the AP B_{max}	100 J
The maximum battery of IoT devices b_{max}	50 mJ
Solar panel size Φ	15 cm ²
Solar energy conversion efficiency $\bar{\eta}$	15%
The maximum transmission power of the AP P_{max}	200 mJ
The mean of the Rayleigh distribution channel μ	1
The variance of the Rayleigh distribution channel σ^2	0.1
Bandwidth of the channel W	20 MHz
Energy requirement per sample \hat{E}	1.38 mJ [23]
User data rate requirement r_{min}	133 Mbps
Total simulated time slots T	150,000
White noise power N_0	10 ⁻⁶ W
Algorithm Parameters	Values
Learning rate α	10 ⁻⁵
Reward decay rate γ	0.4
Number of actions N_A	100
Memory size N_D	50,000
Mini-batch size N_{mb}	200
Updating interval for θ K	Every two slots
Replacing interval for θ' K'	Every 400 slots
Replay start time slot	3,000-th slot
Activation function	leaky ReLU
Initial exploration rate ϵ_0	1
Final exploration rate ϵ_T	0.01
Results collection time	the 120,000-th
Precision of MPC Ψ	10 ⁻³¹
Size of training data set D_t	20
GPR kernels	RBF
Number of predicted slots by MPC L	4

We now investigate the energy efficiency η_t of the AP assuming it has no energy constraint; e.g., when it is connected to the grid. We apply Reward-2, namely energy efficiency. From Figure 4, we see that MPC achieves the highest energy efficiency of around 6.5. In terms of DQN and TRL, we notice that energy efficiency increases because the RL agent learns to determine the optimal transmission power over time. Before the 15,000-th slot, the agent has no knowledge of the environment. Hence, as we can see from Figure 4, the energy efficiency achieved by both DQN and TRL agent is only 4.4. After training, the DQN gains the second-best energy efficiency among the tested algorithms, with around 5.8 on average. By contrast, TRL improves energy efficiency to only 5.5. Also, we see that the energy efficiency of TRL is worse

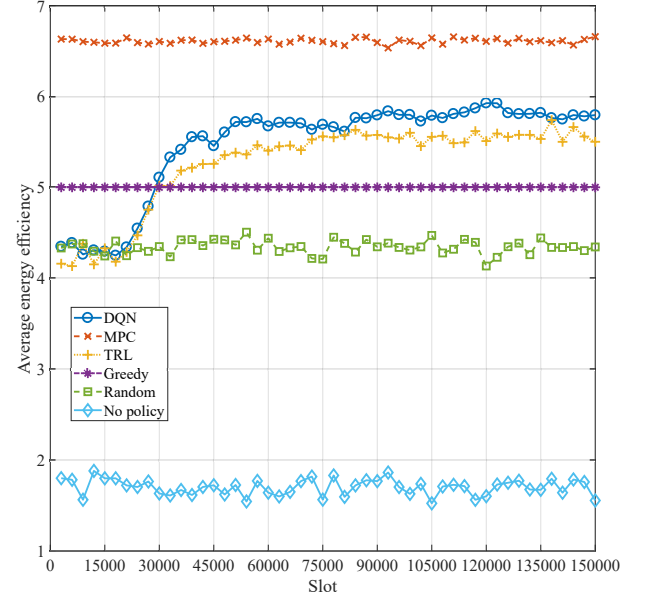


Fig. 4. Elapsed time versus energy efficiency.

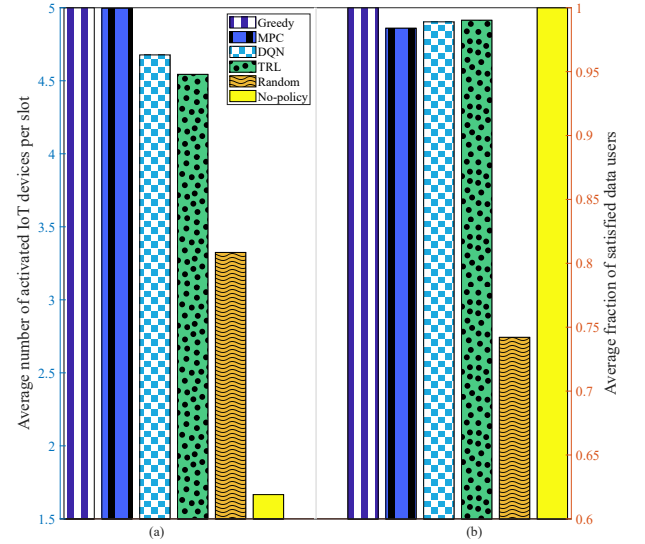


Fig. 5. The satisfaction of both types of users. (a) Average number of activated IoT devices per slot. (b) Average fraction of satisfied data users.

than DQN. This is because DQN takes advantage of neural networks that allow it to deal with continuous and large state space. In our problem, the CSI is random and continuous values, so the state space is large. Also, the memory replay strategy used by DQN breaks the correlation between adjacent states, which helps speed up convergence.

For non-RL approaches, such as Greedy, Random and No-policy, the energy efficiency shown in Figure 4 remains roughly the same. For example, the energy efficiency achieved by Random is always 4.4. This is because the transmission power used by Random is uniformly distributed in the range $[0, 0.2]$ mW, meaning that the average energy consumption per slot/transmission power is 0.1 mW. Such a transmission power level is not sufficient to meet the energy/data rate demands of users. In terms of No-policy, the energy efficiency is around

1.8 because the transmission power used by No-policy is not sufficient to activate every IoT device. As we can see from Figure 5, the number of activated IoT devices is only 1.7

From Figure 5, we see that Greedy has the highest satisfaction for both IoT and legacy data users, with five active devices per slot with a user satisfaction of 100%, respectively. This is because Greedy is able to use the maximum transmit power (200 mW) because there is no energy limitation in this scenario. MPC also achieves almost 100% user satisfaction with five active devices per slot. In terms of data users, MPC achieves a satisfaction value of 0.98. However, from Figure 4, we see that energy efficiency achieved by Greedy is always 5.0, which is lower than MPC by 35%. This means MPC uses 35% less energy to achieve almost the same performance as Greedy. As for DQN, Figure 5 shows that the average number of activated devices per slot is 4.65 and the satisfaction of data users is 0.98. This indicates that MPC performs better than DQN in terms of supporting IoT devices. Also, Figure 4 and 5 indicate that compared to Greedy, DQN support 6% less number of IoT devices per slot but its energy efficiency is 16% higher than Greedy. Lastly, we see that No-policy gains 100% user satisfaction but it only supports 1.7 IoT devices per slot on average. These results confirm that our solutions are able to effectively charge RF-energy IoT devices.

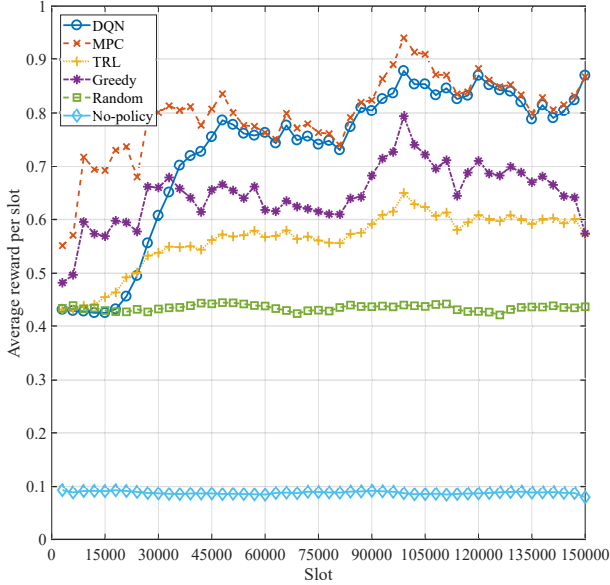


Fig. 6. Elapsed time versus reward gained by the tested algorithms/schemes.

Next, we consider an imperfect energy supply. We set the solar panel size Φ to 15 cm². The energy arrival at the AP is random. Figure 6 shows the satisfaction of both data users and RF-energy devices achieved by the tested algorithms over 150,000 time slots. From Figure 6, we notice that the reward increases significantly because the RL agent learns to use energy over time. Before the 15,000-th slot, the average reward gained by both DQN and TRL agent is only 0.43. After training, the DQN agent gains around 0.8 rewards on average, while TRL improves the reward to only 0.6. Also, we see from Figure 6 that DQN gains around 20% to 30% more reward than TRL. As a result, Figure 7 shows that DQN

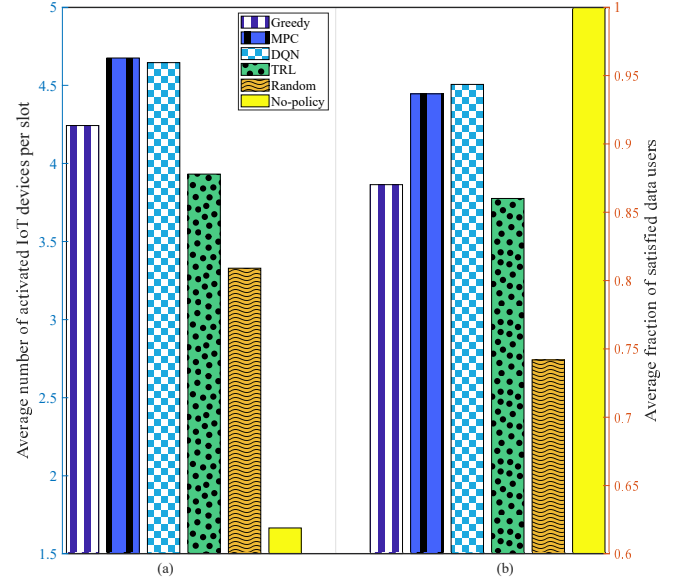


Fig. 7. The satisfaction of both types of users under a random energy arrival scenario. (a) Average number of activated IoT devices per slot, and (b) Average fraction of satisfied data users.

is able to support 20% more IoT devices than TRL, where the number of activated IoT devices achieved by DQN and TRL is 4.61 and 3.9, respectively.

In terms of non-RL algorithms, Figure 6 shows that MPC gains a reward between 0.75 and 0.9 which is the same as the well-trained DQN agent after the 60,000-th slot. MPC also supports 4.65 IoT devices and 0.94 data users per slot on average. We also see that Greedy gains around 0.65 reward on average. However, its performance is worst than the case when the AP has no energy limitation. This is because it does not conserve energy, meaning it causes energy outage. As for the Random rule, from Figure 6, it only gains 0.44 reward on average. This is because Random only uses 0.1 mW energy per slot, leading to battery overflow in around 90% time slots. No-policy gains only 0.1 reward; see Figure 6. The reason is that the number of activated IoT devices achieved by No-policy is only 1.7 per slot on average, meaning IoT devices require more slots to harvest energy until they have sufficient energy to gather a sample. It is worth noting that the performance of DQN and MPC is not significantly affected by random energy arrivals. Comparing Figure 5 and 7, when the AP has imperfect information of its energy arrivals, the user satisfaction of DQN and MPC reduced by around 8% to 4% for both types of users. By contrast, we see from Figure 5 and 7 that the performance achieved by TRL, Greedy and Random drops significantly when we consider random energy arrivals. For example, the average number of activated IoT devices achieved by TRL is 3.9 per slot, whereas it is 4.55 when the AP is powered by a perfect energy source. The reason is that the state space must also include different energy levels at the AP and CSI of users, so the state space is larger. In the case of random energy arrivals, the shortcomings of TRL when for large state space is evident. Moreover, our results show that when we consider an imperfect energy source, transmit power control is critical. The reason is because the AP may encounter

energy shortage, which reduces system performance. This is evident in Figure 5 and 7, the user satisfaction of Greedy and TRL reduces by around 11% to 15%.

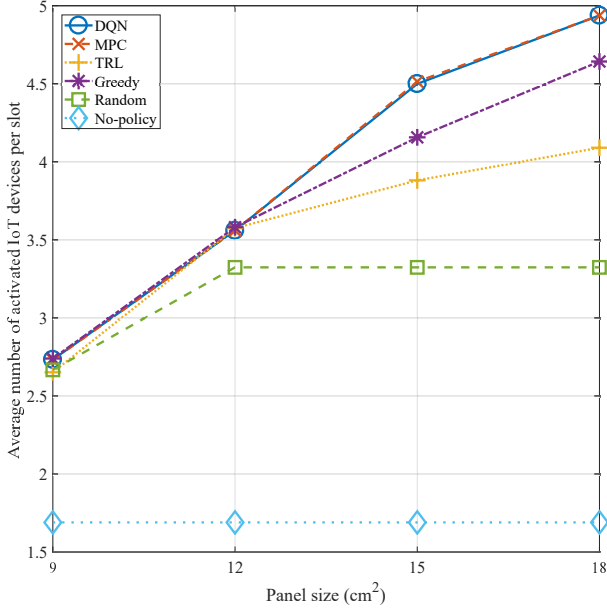


Fig. 8. Varying solar panel sizes versus the number of activated devices.

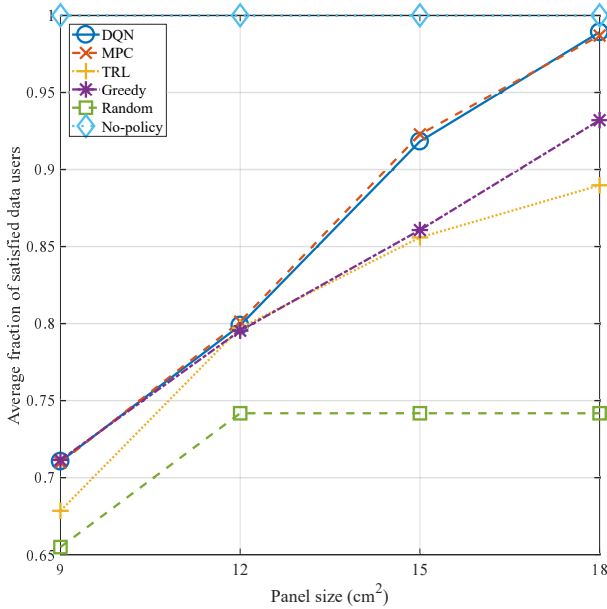


Fig. 9. Varying solar panel sizes versus the fraction of satisfied data users.

Figure 8 and 9 illustrate how different solar panel sizes Φ impact user satisfaction. From Figure 8 and 9, we see that the satisfaction of both types of users increases as the panel size increases. The average number of activated IoT devices of DQN and RMCP increases from 2.75 to 4.9, with a 90% increment as the panel size doubles. Also, the performance of data users increases by 40%, from 0.71 to 0.98. This is because the AP harvests more energy when using a larger solar panel. This allows them to use a higher transmission power to meet the needs of those users that are far away from the AP. In terms

of Greedy and TRL, both of them are able to support 3.55 IoT devices per slot on average, and achieve 80% satisfaction for data users when the solar panel size Φ is 12 cm², see Figure 8 and 9. However, they are inferior to DQN and MPC when Φ is larger than 12 cm². As shown in Figure 8 and 9, the number of activated IoT devices achieved by Random is always 3.3 per slot when the solar panel size is larger than 12 cm². This is because its average energy consumption is 0.1 mW. Moreover, as the solar panel size increases, higher energy arrivals lead to a higher overflow rate. As shown in Figure 8 and 9, the satisfaction of both data users and IoT devices gained by No-policy also remains unchanged as the solar panel size Φ increases. This indicates that the overflow rate of No-policy is higher than other solutions. The number of activated IoT devices is only 1.7. The reason is that the AP is not aware of IoT devices and thus those devices cannot harvest enough energy. Figure 8 and 9 also show that the difference in user satisfaction achieved by different algorithms/schemes is wider as the panel size increases. This means energy management is more necessary when the solar energy arrival rate is large. This is because when the panel size is smaller than 12 cm², the AP is not able to harvest sufficient energy to meet the data/energy requirements of users. By contrast, our DQN and MPC algorithms are able to learn the optimal transmission power to maximize user satisfaction. Therefore, we see that our approaches are significantly superior to the other tested algorithms when the panel size is larger than 15 cm²

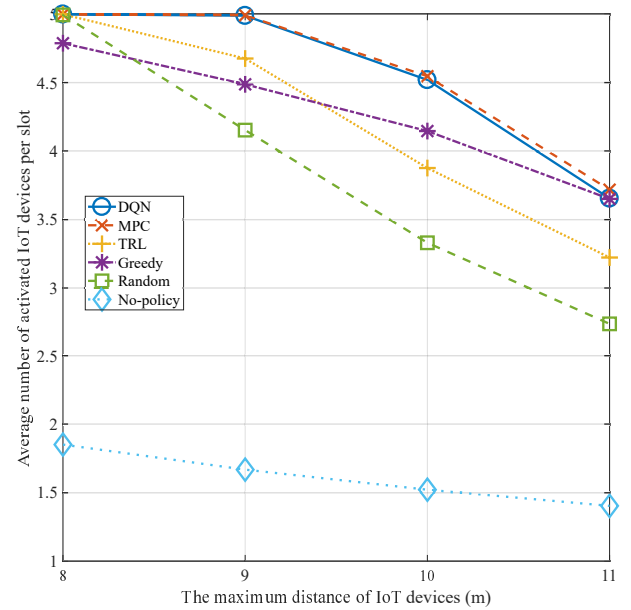


Fig. 10. Average device distance versus the number of activated devices.

We now study different cell sizes. Figure 10 and 11 show that the satisfaction of both types of users decreases by 35% to 45% as the distance/cell size increases. This is because the channel gain becomes smaller if the user distance increases. However, we see that our proposed DQN has minimal degradation in user satisfaction as the cell size becomes larger. For example, the fraction of satisfied data users decreases from 0.98 to 0.87, an 11% drop as the IoT devices distance

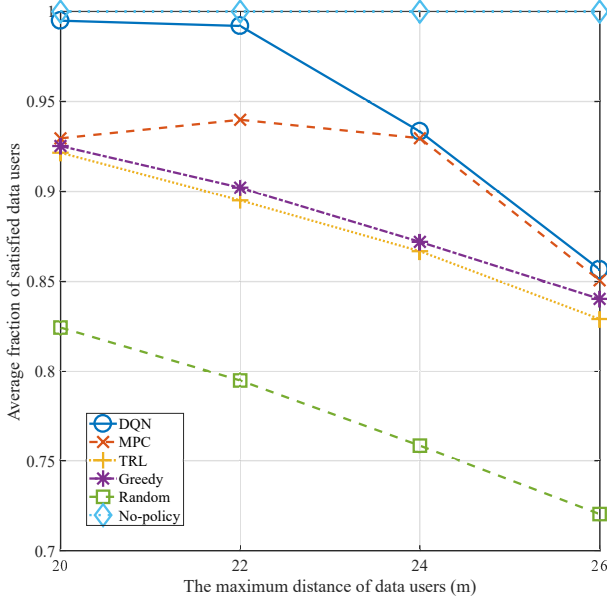


Fig. 11. Maximum user distance versus the fraction of satisfied data users.

increases from 20 to 26 meters. As shown in Figure 11, our DQN algorithm is able to improve the percentage of satisfied data users by 8% to 10% when the maximum user distance is under 24 meters. Figure 10 shows that MPC achieves the same number of activated IoT devices to DQN as the maximum IoT device distance increases from eight to ten meters. However, referring to Figure 11, MPC is no better than DQN in terms of the fraction of satisfied data users, which is the second-best algorithms among the tested algorithms. Figure 11 also shows that as the cell size increases, No-policy supports less RF-energy IoT devices. It only supports 1.4 devices per slot when the maximum IoT device distance is 11 meters. However, the user satisfaction of data users achieved by No-policy is unchanged; see Figure 11. The reason is that No-policy is only aware of data users so it will not increase transmission power if there is energy shortage at IoT devices.

We see from Figure 10 and 11 that the user satisfaction achieved by different tested algorithms converges to a smaller value as user distance increases. For example, in Figure 11, the difference in the fraction of satisfied data users achieved by DQN and MPC converges to 0.01 as the maximum distance of data users increases to 26 meters. This reveals that the AP cannot gain high user satisfaction though transmission power management as the distance increases. The reason is that the channel gain becomes smaller with increasing user/device distance. Consequently, the received power at devices/users is too small for data receptions or energy harvesting no matter what transmission power policy is adopted by the AP.

VI. CONCLUSION

We have shown how an AP can learn to adapt its transmit power when serving data users and simultaneously ensure IoT devices receive sufficient energy. Our work is significant because existing networks will likely be used to support RF-energy harvesting IoT devices. Our results show that the

proposed DQN and MPC algorithms power 10% to 42% more IoT devices and gain 9% to 27% more user satisfaction as compared to approaches without learning capabilities. Also, the results show that our algorithms are able to determine the optimal transmission power for devices and users according to the current and historical battery status.

REFERENCES

- [1] E. Sisinni, A. Saifullah, S. Han, U. Jennehag, and M. Gidlund, "Industrial internet of things: Challenges and opportunities, and directions," *IEEE Transactions on Industrial Informatics*, vol. 14, no. 11, pp. 4724–4735, Nov. 2018.
- [2] V. H. Tran, A. Misra, J. Xiong, and R. K. Balan, "WiWear: Wearable sensing via directional WiFi energy harvesting," in *IEEE International Conference on Pervasive Computing and Communications*, Kyoto, Japan, Mar. 2019.
- [3] C. Hsu, A. Zeitoun, G. He, D. Katabi, and T. Jaakkola, "Self-supervised learning of appliance usage," in *8th International Conference on Learning Representations (ICLR)*, Addis Ababa, Ethiopia, Apr. 2020.
- [4] K. Wang, Y. Wang, Y. Sun, S. Guo, and J. Wu, "Green industrial internet of things architecture: An energy-efficient perspective," *IEEE Communications Magazine*, vol. 54, no. 12, pp. 48–54, Dec. 2016.
- [5] T. Wang, C. Jiang, and Y. Ren, "Access points selection in super WiFi network powered by solar energy harvesting," in *IEEE WCNC*, Doha, Qatar, Apr. 2016, pp. 1–6.
- [6] V. Talla, B. Kellogg, B. Ransford, S. Naderiparizi, S. Gollakota, and J. R. Smith, "Powering the next billion devices with Wi-Fi," in *ACM Conference on Emerging Networking Experiments and Technologies*, Heidelberg, Germany, Dec. 2015.
- [7] X. Lu, P. Wang, D. Niyato, D.-I. Kim, and Z. Han, "Wireless networks with RF energy harvesting: A contemporary survey," *IEEE Communications Surveys Tutorials*, vol. 17, no. 2, pp. 757–767, 2015.
- [8] Q. Sun, G. Zhu, C. Shen, X. Li, and Z. Zhong, "Joint beamforming design and time allocation for wireless powered communication networks," *IEEE Commun. Letters*, vol. 18, no. 10, Oct. 2014.
- [9] H. Ju and R. Zhang, "Throughput maximization in wireless powered communication networks," *IEEE Trans. on Wirel. Commun.*, vol. 13, no. 1, pp. 418–428, Jan. 2014.
- [10] N. Abuzainab, W. Saad, and B. Maham, "Robust bayesian learning for wireless RF energy harvesting networks," in *IEEE WiOpt*, Paris, France, May 2017, pp. 1–8.
- [11] H. Lee and J. Lee, "Resource and task scheduling for SWIPT IoT systems with renewable energy sources," *IEEE Internet of Things Journal*, vol. 6, no. 2, pp. 2729–2748, Apr. 2019.
- [12] H. Ko, S. Pack, and V. C. M. Leung, "Energy utilization-aware operation control algorithm in energy harvesting base stations," *IEEE Internet of Things Journal*, vol. 6, no. 6, pp. 10824–10833, Dec. 2019.
- [13] K. Chin, "On energy and data delivery in wireless local area networks with RF charging nodes," in *ITNAC*, Nov. 2017, pp. 1–7.
- [14] M. Z. Sarwar and K. Chin, "On supporting legacy and RF energy harvesting devices in two-tier OFDMA heterogeneous networks," *IEEE Access*, vol. 6, pp. 62 538–62 551, 2018.
- [15] S. Khairy, M. Han, L. X. Cai, and Y. Cheng, "Sustainable wireless IoT networks with rf energy charging over Wi-Fi (CoWiFi)," *IEEE Internet of Things J.*, vol. 6, no. 6, pp. 10 205–10 218, Dec. 2019.
- [16] M. Ku, Y. Chen, and K. J. R. Liu, "Data-driven stochastic models and policies for energy harvesting sensor communications," *IEEE JSAC*, vol. 33, no. 8, pp. 1505–1520, Aug. 2015.
- [17] F. Alneyadi, M. Alkaabi, S. Alketbi, S. Hajraf, and R. Ramzan, "2.4 GHz WLAN RF energy harvester for passive indoor sensor nodes," in *IEEE International Conference on Semiconductor Electronics*, Kuala Lumpur, Malaysia, Aug. 2014, pp. 471–474.
- [18] R. Bellman, "A markovian decision process," *Journal of Mathematics and Mechanics*, vol. 6, no. 5, pp. 679–684, 1957.
- [19] V. Mnih, K. Kavukcuoglu, D. Silver, A. A. Rusu, J. Veness, M. G. Bellemare, A. Graves, M. A. Riedmiller, A. Fidjeland, G. Ostrovski, S. Petersen, C. Beattie, A. Sadik, I. Antonoglou, H. King, D. Kumaran, D. Wierstra, S. Legg, and D. Hassabis, "Human-level control through deep reinforcement learning," *Nature*, vol. 518, pp. 529–533, 2015.
- [20] L. Yann, B. Yoshua, and H. Geoffrey, "Deep learning," *Nature*, vol. 521, p. 436444, 2015.
- [21] C. K. Williams and C. E. Rasmussen, *Gaussian processes for machine learning*. MIT press, MA, 2006, vol. 2, no. 3.

- [22] L. F. Williams, "A modification to the half-interval search (binary search) method," in *Annual Southeast Regional Conference*, Birmingham, USA, Apr. 1976, p. 95101.
- [23] R. Takitoge, S. Ishigaki, T. Ishige, and K. Ishibashi, "Temperature beat: Persistent and energy harvesting wireless temperature sensing scheme," in *IEEE SENSORS*, Orlando, USA, Oct 2016, pp. 1–3.